LANGMUIR

Article

pubs.acs.org/Langmuir

Ice-Melting Dynamics: The Role of Protons and Interfacial Geometry

Andrew J. Schwartz* and Gerald H. Pollack*

Department of Bioengineering, University of Washington, Box 355061, Seattle, Washington 98195, United States

ABSTRACT: The surface of ice plays a significant role in melting. To better understand the role of the surface, we studied the melting of ice using infrared imaging and pH-sensitive dyes. Ice was allowed to melt in baths of water of varying depths. When the ice melted in a high level of room-temperature water, equal to the height of the ice, the conventional melting pattern appeared. When the ice melted in a chamber with a lower water level, the melting pattern was unexpected. Seconds after the ice was placed in the water, localized regions of low-temperature water appeared around the perimeter of the ice. These regions grew radially outward and seemed to originate as streams coming from inside the ice. Those streams contained high concentrations of protons, as indicated by the color change of a pH-sensitive dye initially placed in the water surrounding the ice. This observation, together with the temperature distribution and ice-shape changes during melting implied that the streams may be propelled by protons from inside the ice. In contrast to conventional melting, which progresses from the outer surface inward, the stream-melting pattern implies a melting process originating inside the ice.

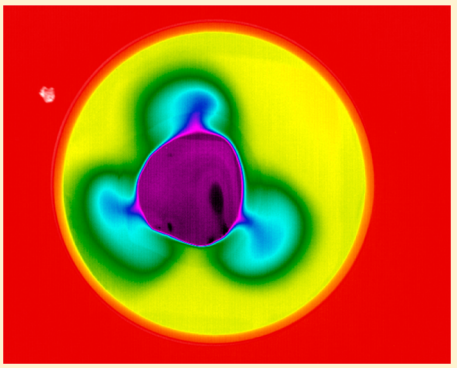

INTRODUCTION

The cyclic freezing and melting of ice in arctic regions largely influences the global weather pattern. Recently, polar ice has been melting at ever-accelerating speed, causing major concerns around the world for sea level rise and elevating temperatures.[1−4] Despite the rapidly changing landscape, it has been difficult to fully understand how the melting ice interacts with the sea around it.[5] In part, this has been due to limited understanding of the process of melting.

It is generally accepted that the water lying on the ice surface is icelike liquid water, having some degree of order. This intermediate-phase water first appears at temperatures below the melting point of ice.[11] Quasi-liquid, premelt, transition layer, icelike liquid, and proton-ordered layer are all terms used to describe that intermediate-phase water, which is found only on the ice surface. How such freshly melted water interacts with surrounding bulk-liquid water remains unclear.

Previous studies have examined melting largely at the ice−air interface.[6−16] By contrast, the interaction of intermediate-phase water with surrounding water is only sparsely studied, with varying results on the thickness of this liquid-like layer.[11,17−20] To understand the nature of the intermediate phase of water, we allowed ice to melt along the solid−liquid interface instead of the solid−air interface.

Another aspect of ice melting is proton order/disorder. In bulk ice, it has been thought that protons are disordered, with high mobility, while on ice surfaces the protons become ordered and immobile.[21−23] Protons are able to move throughout the ice-crystal lattice via transfer to neighboring oxygen atoms. Sequential transfer confers mobility.[23] While proton order has been observed on the ice surface, the involvement of protons in the formation of the intermediate-phase water still remains unclear. A recently discovered intermediate phase of water between solid and liquid, denoted exclusion zone (EZ) water,[24] forms on a wide range of materials and surfaces, while previously discovered intermediate phases are found only on ice surfaces. EZ water offers possible mechanistic insight into the role of protons during ice melting. Thus, experiments were carried out using both infrared imaging to track the associated temperature changes, and pH-sensitive dye to track the dynamics of protons during melting. Some of the results were unexpected.

EXPERIMENTAL PROCEDURES

Ice Preparation. Ice was prepared from 8.0 mL of deionized water (Barnstead, Inc., D3750 Nanopure Diamond Water) pipetted into a plastic Petri dish (BD Falcon, 35 × 10 mm) and then placed in a conventional freezer on a rack at −27 °C for at least 3 h. This process formed cylindrical ice. Dye-containing ice was made from 8.0 mL of phenol-red dye solution (1 mg/mL) using deionized water and frozen as described above.

We also prepared bubble-free ice by placing a large volume of water (1 L) in an open-top square container. Petri dishes (35 × 10 mm) were submerged at the outer edges of this container before the container was frozen at −27 °C overnight. Frozen Petri dishes were carved out from the ice block and ice was extracted from those Petri dish molds. Ice produced in this manner was bubble-free with the same cylindrical shape as the ice described above.

Ice Melting. A larger plastic Petri dish (BD Falcon, 150 × 15 mm) was placed under the infrared camera on a level surface. Forty mL of water at room temperature (20 °C) was added to the Petri dish in the low-water-level experiment, while 150 mL of room-temperature water was added for the high-water-level experiment. The resulting water heights were approximately 0.5 cm for low water level and 1 cm for

Received: January 29, 2017
Revised: May 12, 2017
Published: May 15, 2017

DOI: 10.1021/acs.langmuir.7b00317
Langmuir XXXX, XXX, XXX−XXX

high water level. Ice was taken from the freezer and immediately placed in the center of the water-containing Petri dish. The ice was left to melt in the bath of room-temperature liquid water with an air temperature between 19 and 21 °C. More than 100 experiments were performed in these conditions. In some experiments the water contained pH-sensitive dye (1.0−12.5 μL/mL). Dyes used in these experiments include universal indicator dye, phenol red, congo red, and bromothymol blue. Additional experiments were carried out with varied bath temperatures, either chilled to 10 °C or heated to 30 °C. The melting process was observed with the infrared camera (Figure 1) and recorded.

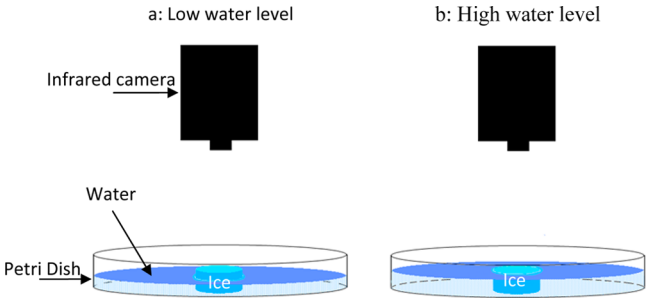

Figure 1. Experimental setup. Low-water-level experiment (a) and high-water-level experiment (b). In the low-water-level configuration, the upper section of the ice remains exposed to air while the bottom rests on the Petri dish. In the high-water-level configuration, the vertical face of ice is covered in water, leaving only the top surface of ice exposed to air. The bottom of the ice floats slightly above the bottom of the Petri dish.

Infrared Imaging. For the experiments, the ice piece was left to melt in a bath of room-temperature liquid water. The following melting processes were recorded at 1 Hz using a FLIR camera with InSb detector (FLIR SC 6000), sensitive within the 3−5 μm range. The camera was positioned 33 cm above the sample. This imaging system can resolve distances of 0.5 mm and measure temperature with an accuracy of ±2% of the reading. ExaminIR software with factory calibration was used for both acquisition and analysis of the data.

Data Analysis. To measure the dynamics of ice melting, video recordings of melting events were analyzed using ExaminIR and ImageJ software. The distance traveled by the freshly melted water over a time interval of typically 10 s was analyzed to compute the velocity of the streams.

Temperature profiles were computed along a line starting from the center of the ice and extending toward the edge of the Petri dish. Measurement along this axis generated a temperature profile. The diameter of the cylindrical ice sample was measured over time to calculate the percent change along various radial axes.

RESULTS

Melting Pattern in High Water. When placed in water at a level slightly higher than the height of the ice, the base of the ice floated slightly above the bottom of the Petri dish. A meniscus formed between the water and the edge of the ice, covering the vertical face up to the top. Only the horizontal flat surface on top of the ice remained exposed to air.

Figure 2 shows the ice-melting process in that configuration, examined with an infrared camera. As the ice melted, a temperature gradient appeared around the ice, with a circularly symmetrical pattern. The temperature of water close to the ice was always lower than that farther from the ice. The ice retained a circular shape throughout melting. This pattern was largely as anticipated.

Around the perimeter of the ice, small "bumps" could be detected, both initially (Figure 2, left, yellow) and later (Figure 2, right, blue). While bumps occasionally persisted throughout melting, individual bumps usually lasted for only a few seconds, were not seen in every experiment, and were not always distributed evenly around the perimeter. Therefore, they were not seen as a significant feature of the melting pattern. On the other hand, they may relate to the stream phenomenon described in low-water-level experiments below.

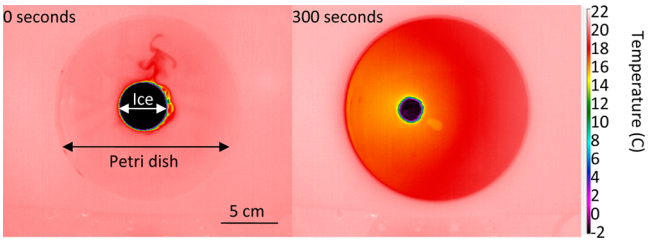

Figure 2. Infrared images of ice and surrounding water in the high-water-level experiment, early (left) and later (right) into melting. Color (scale at right) denotes temperature. The initial upward-pointing finger appearing at 0 s into melting is an artifact arising from placing the ice cube into the water; it quickly dissipated.

Melting Pattern in Low Water. By contrast to the rather conventional pattern seen at high water levels, when ice was placed in the Petri dish with lower water level, melting showed a different pattern (Figure 3). In these experiments, the vertical surface of the ice was approximately half covered in water. Seconds after the ice was placed in the water, well-defined regions of freshly melted water, with lower temperature than the rest of the bath, could be seen growing radially outward from the vertical edges of the ice. We termed these "melting streams". While visible light observation failed to capture this phenomenon, infrared-camera observation showed streams of melted water clearly emerging from the ice. They seemed to burst into the bulk water. Stream melting also occurred in water bath temperatures from 10 to 30 °C.

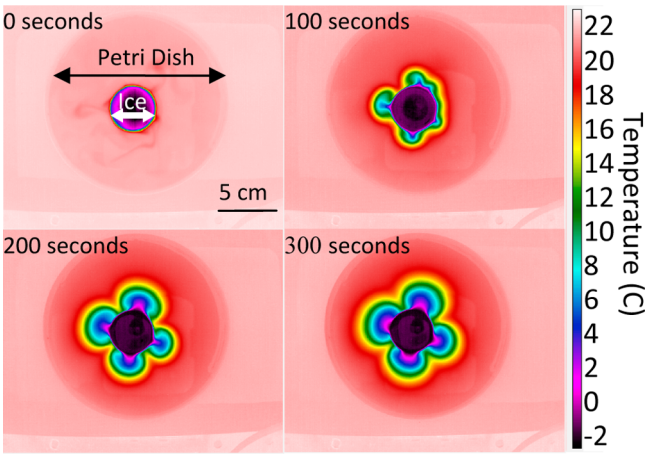

Figure 3. Infrared images of typical stream patterns emerging from ice when placed in low level of water. Color scale at right denotes temperature (°C).

Those streams created the local temperature gradients at several distinct points around the ice surface. No streams could be seen in the areas in between (herein called "nonstreaming" regions). Initial stream velocities were in the range of 100−400 μm/s and decreased over time to zero. Four distinct locations were typical for streams, but 2−8 streams could be observed on

DOI: 10.1021/acs.langmuir.7b00317
Langmuir XXXX, XXX, XXX−XXX

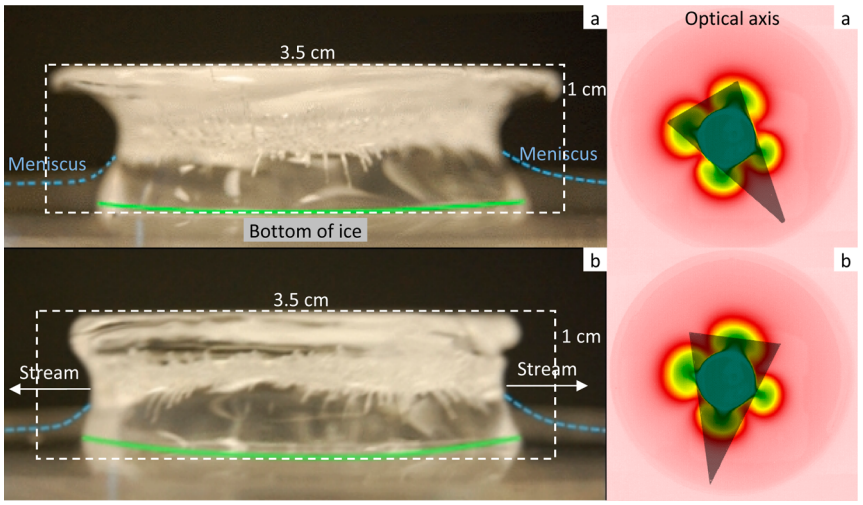

Figure 4. Ice removed from water immediately after undergoing stream melting in low water level for 5 min. The profile view of the nonstreaming ice region (a) shows a large shelf at the top. When rotated to show the stream axis (b), a smaller shelf is seen. Original menisci indicated in blue. White outline shows initial ice shape and dimensions. The infrared images (right) show the respective optical axes.

occasion. At least some of the ice melt came in the form of streams, unlike the patterns seen in the high-water experiment, where water largely enveloped the ice. Further experiments will be needed to precisely quantify the proportion of melting occurring through streams.

Streaming and nonstreaming regions persisted throughout the majority of the melting process. While streams typically reached their maximum extent from the ice surface at ∼300 s, the streams were generally distinguishable from bulk water for up to 20 min into melting and could sometimes persist longer. The generally outward direction of the streams often bent in various directions from the ice surface. Eventually, nearby streams merged as the circumference of the ice diminished.

Shape Changes in Low-Water Experiments. In the low-water-level experiments, on which we focus most of our attention, liquid water formed a meniscus that covered approximately half the height of the ice. This left the upper vertical region exposed to air. In the high-water experiment, by contrast, the meniscus covered the entire (short) vertical face projecting above the water.

The diameter of the top surface of ice, assessed from a top-down view, was measured throughout the melting process. In the high-water experiment, over a period of 300 s, the diameter diminished by 55 ± 8% across all axes. Over the same time period, the low-water experiment showed a much smaller diameter change: 1.8 ± 0.5% along the stream axis and 4.4 ± 0.4% along the nonstream axis. In consequence, the fully submerged ice was observed to melt >3× faster than the partially submerged ice. Thus, fully submerged ice might melt in 20 min, partially submerged ice might melt in >1 h, while ice that was exposed only to air could take up to 4 h to completely melt.

While the difference between stream and nonstream diameter was small, over time this effect led to a progressive loss of the initially circular ice shape; streaming regions retained a larger diameter than the nonstreaming regions. These diameter measurements were taken from a top-down view. An ice shelf always formed from the top layer of ice, demonstrating a minimal melting rate for the ice exposed to air compared to submerged ice (see Figure 4). The shelf blocked the camera's view of the narrowing regions beneath and recorded only the dynamics of the shelf above.

The ice below the shelf was examined through profile views (Figure 4). Color images were used for the profile view, as the infrared imaging system was limited in producing images from a horizontal view. Nonstream regions showed a larger diameter decrease than inferred from the top-down view (Figure 4a). The edges also developed a concave shape. By contrast, the streaming sides of the ice remained flatter (Figure 4b), revealing a diameter change comparable to that of the shelf above.

Bubbles were contained inside of ice, as demonstrated by the white opacity in Figure 5. We carried out additional

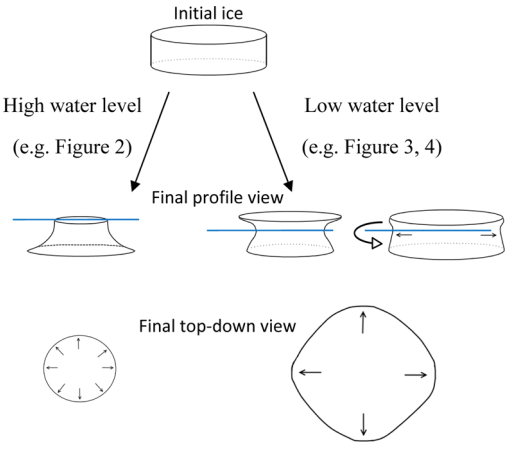

Figure 5. Representative shapes of melted ice. Blue lines indicate approximate water level; arrows inside ice indicate observed flow of water.

experiments on bubble-free ice to examine the effect of bubbles on ice melting. Melting dynamics appeared indistinguishable from the bubble-containing ice, including the presence of stream melting in low water level and nonstream melting in high water level.

Figure 5 schematizes the profiles and top-down views of ice during melting. In both high- and low-water-level experiments, submerged regions of ice were widest at the base and narrowed

DOI: 10.1021/acs.langmuir.7b00317
Langmuir XXXX, XXX, XXX−XXX

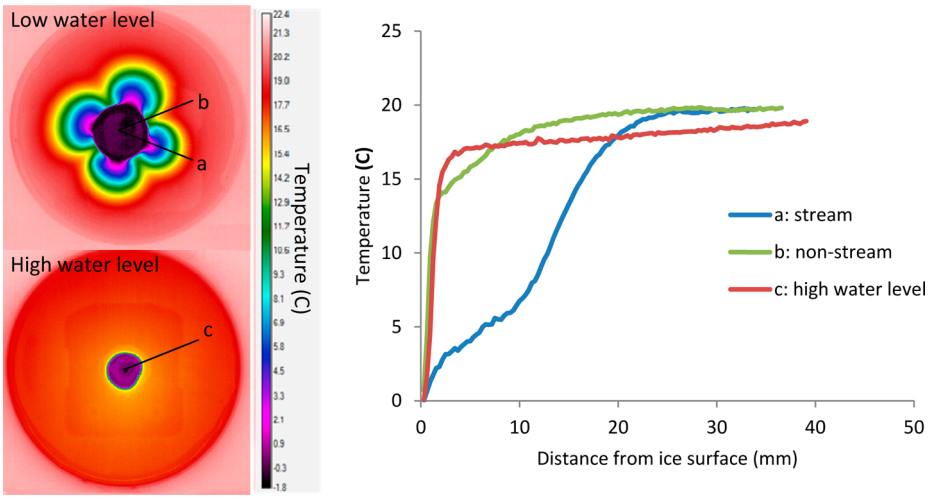

Figure 6. Temperature profiles at 200 s into melting. (Top left) Low-water-level melting. (a) Temperature profile along a stream. (b) Temperature profile along a nonstream region. (Bottom left) High-water-level melting. (c) Temperature profile of high water level. (Right) Composite temperature profiles along the radial axes of the ice from lines a, b, and c. Low-water-level temperature profile is denoted by stream (blue) and nonstream (green) temperature profiles. Red curve, by contrast, denotes high-water-level temperature profile.

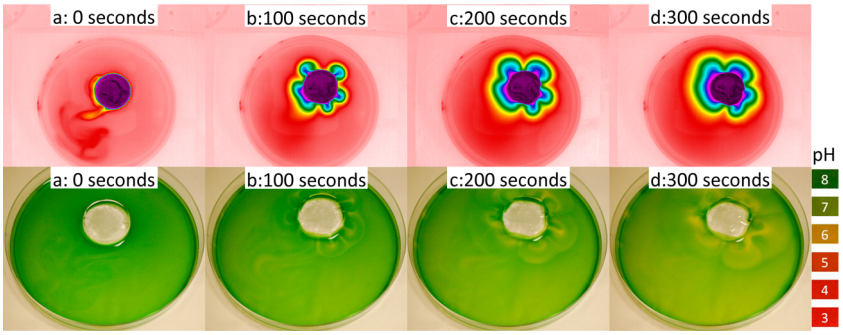

Figure 7. Infrared (top row) and corresponding pH-dye color images (bottom row) of ice in low-level water at various times during melting. pH scale on the right.

toward the water surface. When ice was maximally submerged (Figure 5, left column), the ice formed symmetrical, curved sides. Similarly in low-water-level experiments (Figure 5, right column), submerged ice formed concave sides. However, stream and nonstream regions had different degrees of curvature.

Further, in low-water experiments, ice adopted a polygonal shape during melting. This could be seen from both the profile and top-down views (Figure 5, right column). Ice-emitting streams maintained a larger diameter than nonstream ice as melting progressed. In addition, ice protruding from the surface and exposed to air melted at a negligible rate, adding further asymmetry.

Temperature Profiles. To characterize the melting patterns in more detail, we obtained temperature profiles of the surrounding water (Figure 6). The profiles were obtained along linear axes that spanned from the ice surface into bulk water. In both melting patterns, the temperature of the ice was slightly below 0 °C throughout melting.

In nonstream regions (Figure 6b) and in high-water-level experiments (Figure 6c), temperatures of surrounding water regions increased similarly with distance. The temperature grew from 0 °C at the ice surface to 15 °C 5 mm away, and it rose minimally over the next 40 mm.

By contrast, the temperature profile for the stream-melting regions showed significantly lower temperatures over the same distances (Figure 6a). Temperature increased from 0 °C at the ice surface to 7 °C 15 mm away. From 15 to 30 mm the temperature increased to the bulk-water value. These regions corresponded to the visible streams. Temperature profiles are compared in the graph of Figure 6.

Dye Experiments. Proton concentrations in the water surrounding the melting ice were visualized using pH-sensitive dye (Figure 7). This was used to investigate the proton content of freshly melted streams. Initially, the water surrounding the ice showed a neutral pH (Figure 7a, bottom). When streams became detectable on the infrared images, corresponding streams of clear water appeared in the dye images. Those corresponding stream regions indicated a yellow color after 100 s (Figure 7b), which indicated a lowered pH or a more proton-rich environment. The nonstream regions showed no notable pH change. Note also that the exiting protons eventually turned the bath increasingly yellow, indicating proton accumulation (Figure 7 scale).

The dye patterns also revealed the dynamics of water flow. All movement was in the direction away from the ice, in streams. No dye moved toward the ice for at least the first 300 s of melting. During this time, all of the cold water in the streams emerged from the ice.

For optimized imaging purposes, these images were obtained using pH dye at a concentration of 12.5 μL/mL. Lower concentrations (1.0 μL/mL) and different dyes (see Exper-

DOI: 10.1021/acs.langmuir.7b00317
Langmuir XXXX, XXX, XXX−XXX

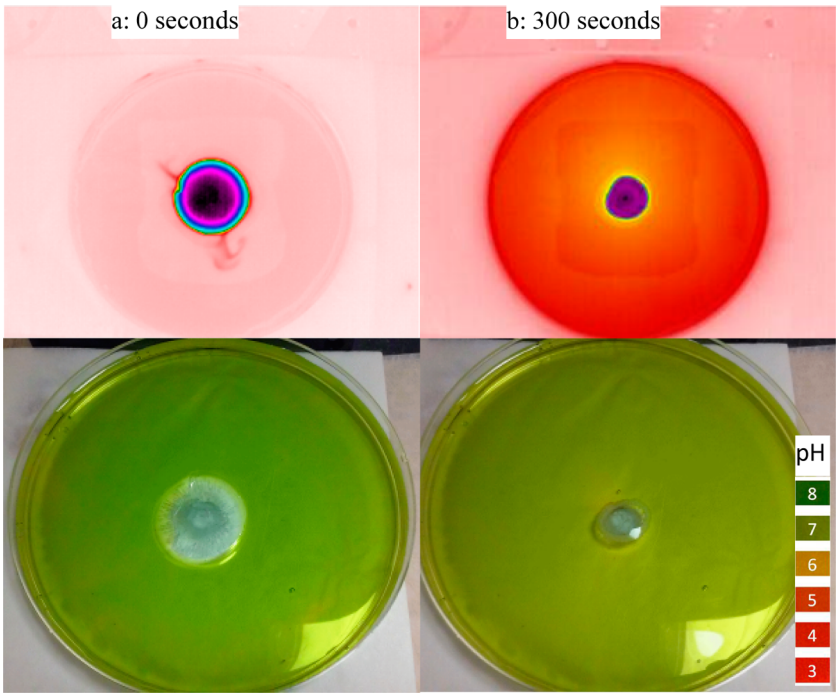

Figure 8. Ice in high level water containing pH dye, at 0 s (left) and 300 s (right) of melting.

imental Procedures) produced similar results. The dye used in these images is a universal dye, sensitive over a pH range of 3–8. While pH dye necessarily alters the properties of the water, no significant impact of the dye's presence was observed on the melting pattern. Streams appeared in a typical fashion in low water level and resulted in ice with a polygonal shape. Similarly, the symmetrical shape of ice in high-water-level melting was unchanged in the presence of dye. Thus, ice-melting dynamics were similar with or without dye.

When the ice melted in high-level water, no such distinctive dye-streaming patterns appeared around the ice. Instead, the water yellowed rather uniformly (Figure 8). Nor was any dye movement observed in high water water, although the dye was observed to move away from the ice in low water level, In both cases, however, it appears that the ice releases low-pH water as it melts.

DISCUSSION

The present experiments were designed to explore the intermediate-phase water formed on the ice surface during melting—a phase that remains poorly understood. In particular, the thickness of the melt layer on the surface of the ice remains uncertain.[11,17−20]

Intermediate-phase water was expected to form at the ice−liquid interface with varying thickness depending on liquid coverage of the ice surface. However, the experiments yielded surprising results. When the surrounding water level was high enough to float the ice, leaving only its top surface exposed, melting proceeded as expected. But when the water level was lower, exposing much of the vertical face of the ice to the air, melting proceeded in an unconventional and unexpected manner: the melt came in the form of proton-rich streams that appeared to emerge from inside the ice. We labeled this feature "stream melting".

The main finding in these experiments is that different melting patterns occur at varying water levels (Figures 2 and 3). Three main features were observed to distinguish these melting patterns: ice geometry, meltwater temperature, and proton efflux. While the exact role of protons in the melting process remains unresolved,[16] protons were observed to be a key feature of melting.

Effects of Surface Coverage on Ice Melting. The key variable in these experiments is the surface coverage of the ice by the surrounding bulk water. Those differences are highlighted in Figure 5. The melting rate in high water level was over three times higher than that in low water level. However, the temperature of the bulk ice was consistent in both melting patterns. Hence, the melting rate appears to be determined mainly by the surface coverage by the surrounding bulk water.

Surface coverage of ice also impacts the shape of the ice. Fully submerged ice formed concave vertical sides and a symmetrical diameter change as it melts. Partially submerged ice melting formed an hourglass shape (Figure 4). Melting along the ice−air interface is negligible. The difference in melting rates between the ice−water and ice−air interfaces gives partially submerged ice an hourglass shape. Melting seems to be largely determined by the ice−water interface.

Shape change or volume loss of the ice does not necessarily indicate melting. Even though substantial ice volume loss occurred in nonstream regions (Figure 4a), meltwater does not emerge from that region. This shape change implies anomalous melting. Regions emitting melted water were expected to incur maximum volume loss. However, the observed shape change indicated that volume loss can occur without meltwater emerging.

Temperature Gradients during Melting. Ice transitions to water through a quasi-liquid melt layer on the ice surface. We attempted to estimate the thickness of this melt layer from temperature measurements (Figure 6). The melt-layer thickness of both nonstreamwater (Figure 6b) and high water level (Figure 6c) extended up to 1 mm from the ice−water interface during the initial melt period. From these results, the thickness

DOI: 10.1021/acs.langmuir.7b00317
Langmuir XXXX, XXX, XXX−XXX

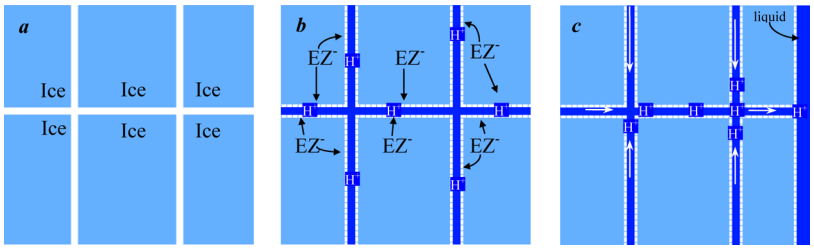

Figure 9. Possible proton movement during melting. Domain boundaries form ice veins in ice (a). As melting initiates (b) EZ water forms (dashed line) near those domain boundaries, filling the interstitial space with low-pH liquid water (dark blue). Repulsion generates outward flow, releasing protons from ice veins into liquid water (c).

of the melt layer does not seem to relate to the ice-melting rate, because high water level melts up to three times faster than nonstream regions; yet, over the initial melt period, the melt layer seems to have the same thickness. On the other hand, stream melting seemed to extend the melt layer up to 10 mm from the ice surface, where the water temperature diminished (Figure 6a).

Temperature gradients further distinguish stream melting and conventional melting. The temperature pattern in high water level indicated that melting arose primarily because of the higher temperature of the surrounding water. The melted ice appeared to diffuse directly from the ice surface into bulk water (Figure 2).

By contrast, low-water-level melting created the stream pattern. Stream temperatures remained much lower than nearby bulk water temperatures at great distances from the ice surface (Figures 3 and 6). The finding of low stream temperature supports the notion that streams are mainly composed of freshly melted water.

Proton Efflux during Melting. It has been suggested that melting produces an increase in proton concentration in the freshly melted water.[24] While the high- and low-water experiments yielded different melting patterns, in both cases the freshly melted water had lower pH compared to bulk water (Figures 7 and 8). It is possible that the pH dye used to measure the proton content of freshly melted water interferes with the melting process. However, whatever interference may have occurred had a negligible impact on the observed melting pattern, as stream and conventional melting occurred in much the same way with or without dye. Furthermore, the melting rate in both situations remained unchanged. Hence, the results appear to indicate low-pH effluent as a consistent feature of the melting process. The various theories on intermediate-phase water, which include premelt layers,[6−16] EZ water,[24,25] and theories on ice veins and domain structure of ice,[26−28] suggest a mechanism for the general appearance of protons in meltwater. This seems confirmed.

The released protons may come from the premelt layers that form on the ice surface prior to melting. In those surface layers the protons are immobile.[21−23] Said protons could emerge in the liquid water that melts from those surface layers. Further, the highly mobile protons in the underlying bulk ice could become immobilized as they transition to new premelt layers, subsequently emerging into the bulk water. In configurations with streams, the protons aggregate into streams prior to emerging into bulk water. The process of melting through premelt layers ensures that the melting surface is saturated with protons.

Exclusion zone (EZ) theory further supports the increased protons observed in freshly melted water.[24] In this construct, ice forms from negatively charged EZ water and positively charged protons. Formation of EZ water from bulk water is the first phase of the freezing transition. During the second phase, protons bind to EZ water, forming ice. The opposite occurs during melting. The first step of melting is the separation of protons from the ice lattice. This separation yields EZ water and low-pH liquid water,[25] whose protons can diffuse into the bulk water. Thus, EZ water acts as an intermediate phase between solid and liquid water. Proton release always occurs during the transition of ice to EZ water in the form of low-pH water. This fits the observation that low pH was consistently observed in freshly melted water.

Eventually, EZ water transitions into liquid water as it recombines with protons. However, the fact that EZ water is structurally similar to ice may allow the EZ to remain associated with the rest of the ice lattice even as protons are ejected. This allows EZ water to persist as an intermediate layer of ice over the initial phases of melting, when stream melting is most active. During this period, the ice-to-EZ transition can generate enough protons to propel streams outward. As the bulk water receives these protons, its capacity to draw low-pH water from streams may reach a limit, thereby slowing the process.

Ice veins provide a mechanism for the origin of streams (Figure 9). Ice veins surround each domain that composes the bulk ice (Figure 9a). They form a network, extending from within the bulk ice to the ice surface. They are known to retain high concentrations of ions, including protons.[26−28] Melting along the domain boundaries produces intermediate-phase water at the boundaries lining those veins (Figure 9b). As intermediate phases form, protons are released into the veins, as previously described. A sufficient accumulation of proton-rich water may then create a repulsive force that self-propels through those veins, emerging from the ice surface as streams (Figure 9c).

Thus, streams appear when ice-vein contents generate enough repulsive force. On the other hand, when the ice melts sufficiently rapidly, as in high water level, ice veins may not have time to build enough repulsive force; thus, streams may not occur. However, small bumps, which resembled streams, did appear in those high-water-level experiments, indicating the possibility of some repulsive force limited to localized ice regions. Aggregation of protons in ice veins may also lead to the polygonal geometry seen in ice melting in low water level. The low-pH water that exits the ice during stream melting can be replenished by meltwater generated from nearby ice veins. A directional flow of meltwater toward the stream region is then established. Ice-melting rate may vary in different regions depending of the efflux of meltwater, leading to a polygonal shape.

DOI: 10.1021/acs.langmuir.7b00317
Langmuir XXXX, XXX, XXX−XXX

CONCLUSION

Stream melting sharply contrasts with conventional melting. This unusual melting pattern shows that ice has various melting modes. Conventionally, melting is considered to occur from the surface inward, and this process is determined by temperature and pressure. Stream melting shows that ice geometry, intermediate-phase water, and protons may play a role in the melting process.

These features could have a large impact on the understanding of ice at larger scales. For example, charge separation occurs during melting. The cyclical freezing and melting of polar ice may lead to an accumulation of protons and other ions. Ionization is critical in geological[29] and atmospheric[30] issues. Understanding the mechanisms of large-scale ion release could be a significant step in developing a capacity to manage that issue.

Another feature of melting that we examined was the nature of the ice−water interface. While melting at the ice−air interface is negligible, a dynamic melting process occurs at the ice−water interface. These findings provide a new approach to quantifying the proportion of ice melt resulting from ice−water and ice−air interactions. More accurate predictions of polar ice melt and its consequences can be made based on ice−water surface coverage.

AUTHOR INFORMATION

ORCID

Andrew J. Schwartz: 0000-0001-9999-3302

Notes

The authors declare no competing financial interest.

REFERENCES

(1) Church, J. A.; Clark, P. U.; Cazenave, A.; Gregory, J. M.; Jevrejeva, S.; Levermann, A.; Merrifield, M. A.; Milne, G. A.; Nerem, R. S.; Nunn, P. D.; Payne, A. J.; Pfeffer, W. T.; Stammer, D.; Unnikrishnan, S. Sea Level Change. In *Climate Change 2013: The Physical Science Basis. Contribution of Working Group I to the Fifth Assessment Report of the Intergovernmental Panel on Climate Change*; Stocker, T. F., Qin, D., Plattner, G.-K., Tignor, M., Allen, S. K., Boschung, J., Nauels, A., Xia, Y., Bex, V., Midgley, P. M., Eds.; Cambridge University Press: Cambridge, U. K. and New York, 2013.

(2) Vermeer, M.; Rahmstorf, S. Global sea level linked to global temperature. *Proc. Natl. Acad. Sci. U. S. A.* **2009**, *106* (51), 21527−21532.

(3) Radic, V.; Bliss, A.; Beedlow, A. C.; Hock, R.; Miles, E.; Cogley, J. G. Regional and global projections of twenty-first century glacier mass changes in response to climate scenarios from global climate models. *Climate Dynamics.* **2014**, *42* (1), 37−58.

(4) Bamber, J.; Riva, R. The sea level fingerprint of recent ice mass fluxes. *Cryosphere.* **2010**, *4*, 621−627.

(5) Csatho, B. M.; Schenk, A. F.; van der Veen, C. J.; Babonis, G.; Duncan, K.; Rezvanbehbahani, S.; van den Broeke, M. R.; Simonsen, S. B.; Nagarajan, S.; van Angelen, J. H. Laser altimetry reveals complex pattern of Greenland Ice Sheet dynamics. *Proc. Natl. Acad. Sci. U. S. A.* **2014**, *111* (52), 18478−18483.

(6) Park, K.; Lin, W.; Paesani, F. Fast and Slow Proton Transfer in Ice: The Role of the Quasi-Liquid Layer and Hydrogen-Bond Network. *J. Phys. Chem. B* **2014**, *118*, 8081−8089.

(7) Lipowsky, R. Critical surface Phenomena at First-Order Bulk Transitions. *Phys. Rev. Lett.* **1982**, *49*, 1575−1578.

(8) Nason, D.; Fletcher, N. H. Photoemission from ice and water surfaces: Quasiliquid layer effect. *J. Chem. Phys.* **1975**, *62*, 4444−4449.

(9) Wei, X.; Miranda, P. B.; Shen, Y. R. Surface Vibrational Spectroscopic Study of Surface Melting of Ice. *Phys. Rev. Lett.* **2001**, *86*, 1554−1557.

(10) Golecki, I.; Jaccard, C. Intrinsic surface disorder in ice near the melting point. *J. Phys. C: Solid State Phys.* **1978**, *11*, 4229−4237.

(11) Lied, A.; Dosch, H.; Bilgram, J. H. Surface Melting of ice I_h Single Crystals Revealed by Glancing Angle X-ray Scattering. *Phys. Rev. Lett.* **1994**, *72*, 3554−3557.

(12) Dosch, H.; Lied, A.; Bilgram, J. H. Disruption of the hydrogen-bonding network at the surface of I_h ice near surface premelting. *Surf. Sci.* **1996**, *366*, 43−50.

(13) Ikeda-Fukazawa, T.; Kawamura, K. Molecular-dynamics studies of surfaces of ice Ih. *J. Chem. Phys.* **2004**, *120*, 1395−1401.

(14) Li, Y.; Somorjai, G. A. Surface Premelting of Ice. *J. Phys. Chem. C* **2007**, *111*, 9631−9637.

(15) Bishop, C. L.; Pan, D.; Liu, L. M.; Tribello, G. A.; Michaelides, A.; Wang, E. G.; Slater, B. On thin ice: surface order and disorder during pre-melting. *Faraday Discuss.* **2009**, *141*, 277−292.

(16) Frenken, J. W.; Marée, P. M.; van der Veen, J. F. Observation of surface-initiated melting. *Phys. Rev. B: Condens. Matter Mater. Phys.* **1986**, *34*, 7506−7516.

(17) Beaglehole, D.; Nason, D. Transition layer on the surface on ice. *Surf. Sci.* **1980**, *96*, 357−363.

(18) Dosch, H.; Lied, A.; Bilgram, J. H. Glancing-angle X-ray-scattering studies of the premelting of ice surfaces. *Surf. Sci.* **1995**, *327*, 145−164.

(19) Doppenschmidt, A.; Butt, H. J. Measuring the thickness of the liquid-like layer on ice surfaces with atomic force microscopy. *Langmuir* **2000**, *16*, 6709−6714.

(20) Bluhm, H.; Ogletree, D. F.; Fadley, C. S.; Hussain, Z.; Salmeron, M. The premelting of ice studied with photoelectronspectroscopy. *J. Phys.: Condens. Matter* **2002**, *14* (8), L227−L233.

(21) Brown, D. E.; George, S. M. Surface and Bulk Diffusion of $H_2{}^{18}O$ on Single-Crystal $H_2{}^{16}O$ Ice Multilayers. *J. Phys. Chem.* **1996**, *100*, 15460−15469.

(22) Buch, V.; Groenzin, H.; Li, I.; Shultz, M. J.; Tosatti, E. Proton order in the ice crystal surface. *Proc. Natl. Acad. Sci. U. S. A.* **2008**, *105* (16), 5969−5974.

(23) Cowin, J. P.; Tsekouras, A. A.; Iedema, M.J.; Wu, K.; Ellison, G. B. Immobility of protons in ice from 30 to 190 K. *Nature* **1999**, *398*, 405−407.

(24) Pollack, G. H. *The Fourth Phase of Water*; Ebner and Sons: Seattle, WA, 2013.

(25) So, E.; Stahlberg, R.; Pollack, G. H. Exclusion zone as an intermediate between ice and water. *WIT Trans. Ecol. Environ.* **2011**, 3−11.

(26) Barletta, R. E.; Priscu, J. C.; Mader, H. M.; Jones, W. L.; Roe, C. H. Chemical analysis of ice vein microenvironments: II. Analysis of Glacial samples from Greenland and Anatarctica. *J. Glaciol.* **2012**, *58* (212), 1109−1118.

(27) Nye, J. F. The Geometry of Water Veins and Nodes in Polycrystalline Ice. *J. Glaciol.* **1989**, *35* (119), 17−22.

(28) Jenniskens, P.; Banham, S. F.; Blake, D. F.; McCoustra, M. R. S. Liquid water in the domain of cubic crystalline ice I c. *J. Chem. Phys.* **1997**, *107* (4), 1232−1241.

(29) Albright, R.; Caldeira, L.; Hosfelt, J.; Kwiatkowski, L.; Maclaren, J. K.; Mason, B. M.; Nebuchina, T.; Ninokawa, A.; Pongratz, J.; Ricke, K. L.; Rivlin, T.; Schneider, K.; Sesboüé, M.; Shamberger, K.; Silverman, J.; Wolfe, K.; Zhu, K.; Caldeira, K. Reversal of ocean acidification enhances net coral reef calcification. *Nature* **2016**, *531*, 362−365.

(30) Solomon, S. Progress towards a quantitative understanding of Antarctic ozone depletion. *Nature* **1990**, *347*, 347−354.

DOI: 10.1021/acs.langmuir.7b00317
Langmuir XXXX, XXX, XXX−XXX